Polarimetry: From the Sun to Stars and Stellar Environments
Proceedings IAU Symposium No. 305, 2014
K. N. Nagendra, S. Bagnulo, R. Centeno &
M. J. Martínez González, eds.

doi:10.1017/S1743921315004664

Coherence structure of D_1 scattering

Jan Olof Stenflo[1,2]

[1]Institute of Astronomy, ETH Zurich, CH-8093 Zurich, Switzerland
[2]Istituto Ricerche Solari Locarno, Via Patocchi, CH-6605 Locarno Monti, Switzerland
email: stenflo@astro.phys.ethz.ch

Abstract. The extensive literature on the physics of polarized scattering may give the impression that we have a solid theoretical foundation for the interpretation of spectro-polarimetric data. This theoretical framework has however not been sufficiently tested by experiments under controlled conditions. While the solar atmosphere may be viewed as a physics laboratory, the observed solar polarization depends on too many environmental factors that are beyond our control. The existence of a symmetric polarization peak at the center of the solar Na D_1 line has remained an enigma for two decades, in spite of persistent efforts to explain it with available quantum theory. A decade ago a laboratory experiment was set up to determine whether this was a problem for solar physics or quantum physics. The experiment revealed a rich polarization structure of D_1 scattering, although available quantum theory predicted null results. It has now finally been possible to formulate a well-defined and self-consistent extension of the theory of quantum scattering that can reproduce in great quantitative detail the main polarization structures that were found in the laboratory experiment. Here we give a brief overview of the new physical ingredients that were missing before. The extended theory reveals that multi-level atomic systems have a far richer coherence structure than previously believed.

Keywords. line: profiles, methods: laboratory, atomic processes, polarization, radiation mechanisms: general, scattering, Sun: atmosphere

1. Introduction

Systematic exploration of the Second Solar Spectrum (the linearly polarized spectrum that is exclusively caused by coherent scattering processes) became possible two decades ago through the introduction of the ZIMPOL technology, which allowed imaging polarimetry with a precision of 10^{-5} in the degree of polarization (Povel 1995, 2001; Gandorfer et al. 2004). Among the wealth of previously unknown polarization features, the symmetric polarization peak in the core of the well-known Na I D_1 line at 5896 Å was immediately recognized as enigmatic (Stenflo & Keller 1996, 1997), because the D_1 transition was believed to be intrinsically unpolarizable. Numerous attempts have been made to explain the observed D_1 behavior (as documented in greater detail in Stenflo *et al.* 2000a,b) in terms of optical pumping of the hyperfine structure levels of the ground state or as caused by the spectral structuring of the solar D_1 radiation, but they have all failed either because the predicted amplitude has been much too small, or because the predicted polarization profile has been anti-symmetric rather than having the observed symmetric shape (Landi Degl'Innocenti 1998; Trujillo Bueno *et al.* 2002; Casini *et al.* 2002; Kerkeni & Bommier 2002; Klement & Stenflo 2003; Casini & Manso Sainz 2005; Belluzzi & Trujillo Bueno 2013).

Even if there were potentially promising or apparently successful attempts to explain the solar observations, they could hardly be conclusive, since the solar atmosphere represents a 'messy' laboratory beyond our control. It is full of tangled, spatially unresolved magnetic fields, it is optically thick with multiple scattering in unresolved

multi-dimensional geometries, and so on. The only way to obtain a clear answer to the question whether the D_1 enigma is a problem of solar physics or of quantum mechanics is to experimentally study D_1 scattering under controlled conditions in a terrestrial laboratory.

Experiments with polarized scattering played a key role in the early development of quantum mechanics. The work by Wilhelm Hanle in Göttingen (Hanle 1924) for instance demonstrated the concept of coherent superposition of quantum states and the partial decoherence caused by external magnetic fields, a phenomenon that is widely used in different areas of physics under the name 'Hanle effect'. The literature on experiments with polarized scattering however came to a sudden end around 1935, apparently because the field was considered to be exhausted.

Because the weak polarization effects of D_1 scattering that we are concerned with now were far beyond reach with the technology available in 1935, it happened that this domain of quantum physics never got experimentally tested. Still this highly complex theory is continually being used in this untested domain. A decade ago we therefore set up a laboratory experiment to explore the basic physics of D_1 90° scattering under the simplest possible, well-defined conditions. The experiment and its main results have been described in detail by Thalmann *et al.* (2006, 2009).

The available theory for quantum scattering failed the laboratory test! The observed D_1 scattering was found to have a rich polarization structure where the theory predicted null results. This immediately raised the question how the theory would need to be changed or extended to explain the experimental data. We can now finally identify the physical ingredients that have been missing and present a self-consistent extension of quantum scattering theory, which is able to reproduce the D_1 results in great quantitative detail while avoiding the use of adjustable free parameters (because we fix the model parameters through fits to the D_2 results, without reference to D_1).

A detailed account of the procedure used to extend quantum scattering theory has recently been given in Stenflo (2015). Here we give a highly condensed presentation of the physics that is involved.

2. Brief overview of the theory of polarized scattering

2.1. *Scattering probability amplitudes*

The probability amplitude for scattering from initial magnetic substate labeled a to final substate f via intermediate substate b is given by the Kramers-Heisenberg expression

$$w_{\alpha\beta} \sim \langle f \,|\, \hat{\mathbf{r}} \cdot \mathbf{e}_\alpha \,|\, b \rangle \langle b \,|\, \hat{\mathbf{r}} \cdot \mathbf{e}_\beta \,|\, a \rangle \, \Phi_{ba} \,, \tag{2.1}$$

with

$$\Phi_{ba} = \frac{2/i}{\omega_{ba} - \omega - i\gamma/2}, \tag{2.2}$$

being the area-normalized absorption profile function, while ω_{ba} is the resonant absorption transition frequency and ω is the frequency of the incident radiation field (for a given monochromatic Fourier component, cf. Stenflo 1994, 1998).

The matrix elements in Eq. (2.1) can be conveniently expressed as products between two factors. One purely geometrical factor, for which we use symbol ε, represents the scalar product between the complex spherical base vectors of the atomic system and the real linear polarization base vectors in the transverse plane of the radiation. The other factor is the probability amplitude t for the transition between two sublevels. Then we can write

$$w_{\alpha\beta} \sim \Phi_{ba} \, \varepsilon_{q'}^{\alpha *} \, \varepsilon_q^\beta \, t_{fb} \, t_{ba} \,. \tag{2.3}$$

https://doi.org/10.1017/S1743921315004664 Published online by Cambridge University Press

Indices q and q' represent the difference between the lower and upper magnetic quantum numbers and have values 0, ± 1.

For an atomic system with hyperfine structure splitting in the Paschen-Back regime (which is the case for the D_1 lines of Na I, K I, Li I, and Ba II), the probability amplitudes t and the transition frequencies ω_{ba} depend on the magnetic field in a non-linear way, but the factorization in Eq. (2.3) remains valid.

A classical oscillator corresponds to the case of a $J = 0 \rightarrow 1 \rightarrow 0$ scattering transition, for which $q = q'$ and $a = f$. Because the t amplitudes are the same for each of the three component oscillators (that represent the three spatial degrees of freedom), they are not needed in the classical expression for the scattering probability amplitude.

Let us stress that we have no reason to question the way in which probability amplitudes are calculated in quantum mechanics. The problems arise when we want to calculate probabilities (which represent the observables) from the probability amplitudes, i.e., when we go from the 2×2 complex Jones-type matrix $\mathbf{w}$ with components $w_{\alpha\beta}$ to the complex 4×4 coherency matrix $\mathbf{W}$, which has the same physical contents as the Mueller matrix $\mathbf{M}$ that describes scattering of the Stokes vector, as seen from the relation

$$\mathbf{M} = \mathbf{T}\,\mathbf{W}\,\mathbf{T}^{-1}\,, \tag{2.4}$$

where the complex 4×4 matrices $\mathbf{T}$, $\mathbf{T}^{-1}$ are purely mathematical transformation matrices without physical contents (cf. Stenflo 1994).

2.2. *Coherent summation over the initial and final states*

The standard recipe for the derivation of scattering probabilities from probability amplitudes is based on the concept 'sum over histories': For given, fixed initial and final states a and f one first sums the probability amplitudes for all the possible ways (i.e., for all the possible intermediate states b) in which one can go from a to f. The probability to go from a to f is then obtained by forming the product between such a sum and its complex conjugate. To get the total scattering probability when there are many different substates a and f one then adds up the probabilities for the various a-f combinations, weighted by the relative populations $|\,c_a|^2$ of the different initial a states (where c_a is the complex probability amplitude for substate a). With this recipe all the coherences originate from interferences (cross products) between alternative histories, i.e., between different intermediate states.

In the polarization case the probability amplitudes are represented not by scalar functions but by complex 2×2 matrices $\mathbf{w}$ with components $w_{\alpha\beta}$. The product between the probability amplitude and its complex conjugate then becomes a tensor product $\otimes$, leading to the complex 4×4 coherency matrix $\mathbf{W}$ that represents the scattering probabilities. In explicit form we then get

$$\mathbf{W} = \sum_a |\,c_a|^2 \sum_f \Big(\sum_b \mathbf{w} \Big) \otimes \Big(\sum_{b'} \mathbf{w}^* \Big)\,. \tag{2.5}$$

This expression highlights the fundamentally different ways in which the three types of atomic states are treated: the summation over the intermediate substates b is coherent (done over the probability amplitudes), while the summations over the initial and final substates a and f is incoherent (done outside the tensor product, over the probabilities).

With this computational recipe quantum mechanics predicts null results for scattering of linearly polarized light at a D_1 type atomic transition, in glaring contradiction with our laboratory experiment for potassium D_1 scattering, which reveals a rich polarization structure of the scattered radiation.

https://doi.org/10.1017/S1743921315004664 Published online by Cambridge University Press

We have found that nearly perfect agreement between theory and experiment can be obtained if we remove the distinction between coherent and incoherent summations and make all of them coherent. This implies that the correct way to calculate the coherency matrix should instead be

$$\mathbf{W} \;=\; \Big(\sum_{abf} c_a\,\mathbf{w}\Big) \otimes \Big(\sum_{a'b'f'} c^*_{a'}\,\mathbf{w}^*\Big)\,. \tag{2.6}$$

This expression opens the door for atomic systems to have a far richer coherence structure than is possible with Eq. (2.5), which excludes the main interference terms that we now find are the ones that govern the outcome of the laboratory experiment.

2.3. *Coherences in the initial state*

There is a common misconception that atomic transitions occur as instantaneous quantum jumps, when in fact they take a very long time, about 10 million times longer than the oscillation period of the electric vector of the radiation field. Wave packets that represent photons before they reach a detector are huge objects. The coherence length of wave packets emitted from potassium D_1 and D_2 is about 8 m, the distance that light travels during the radiative damping time. Each single wave packet therefore represents a radiation bath, in which the atomic dipole moment is being shaken by the oscillating electric field about 10 million times during the interaction event.

In contrast the traditional scenario for optical pumping is a sequence of discrete, nearly instantaneous transition events, because the theory is only available under the assumption of the 'flat spectrum approximation' (cf. p. 257 in Landi Degl'Innocenti & Landolfi 2004). According to Heisenberg's uncertainty principle and basic Fourier theory, broader spectral band width means shorter coherence length. The interaction with broad-band wave packets would therefore be nearly instantaneous, but such wave packets do not occur in nature.

Both the lower and upper levels of the D_1 transition are split into hyperfine states with quantum numbers $F = 1$ and 2, which have 3 and 5 magnetic substates, respectively. There are 36 allowed electric dipole transitions between the 8 lower and 8 upper substates.

We can conceptually think of the allowed resonant transitions as 36 elastic strings (like the strings in a musical instrument), which are being excited together while immersed in the radiation bath of the wave packet. The strings are linked with each other in a network: different strings share the same end points. Since the entire network is being driven by a common oscillating electric field, the phases of the different oscillating strings get synchronized. It is this process that generates the coherences $c_a\,c^*_{a'}$ (off-diagonal elements of the density matrix) in the initial state.

Among the various types of coherences that are allowed in the extended theory of Eq. (2.6), the only one that is also allowed by the old recipe of Eq. (2.5) is the interference between the two profile functions Φ_{ba} (although Eq. (2.5) also has the restriction that $a' = a$, in contrast to Eq. (2.6)). The product of two such profile functions can be expressed as a product between one frequency-independent part that describes the decoherence due to the different resonant frequencies, and one frequency-dependent part that integrates to unity (since each profile function is area-normalized):

$$\Phi_{ba}\,\Phi^*_{b'a'} \;\sim\; \cos\alpha\; e^{i\alpha}\;\tfrac{1}{2}\,(\Phi_{ba} + \Phi^*_{b'a'}), \tag{2.7}$$

(cf. Stenflo 1994, 1998). The angle α given by

$$\tan\alpha = \frac{\omega_{ba} - \omega_{b'a'}}{\gamma}\,, \tag{2.8}$$

is usually referred to as the 'Hanle angle' when the frequency splitting is caused by

https://doi.org/10.1017/S1743921315004664 Published online by Cambridge University Press

magnetic fields (Zeeman splitting). The expressions are however valid regardless of the physical origin of the splitting.

Each initial substate amplitude c_a oscillates like $\exp(-iE_a\,t/\hbar)$. In the absence of an external radiation field the phases of different substates quickly randomize, causing the ensemble averages of the off-diagonal density matrix elements $c_a c_{a'}^*$ to vanish. The radiation bath provided by each wave packet however drives the oscillations of the linked string network to induce phase synchronization between the different substates, causing $c_a c_{a'}^*$ to oscillate like $\exp(-i\,\omega_{aa'}\,t - \gamma\,t)$, which is damped because the driving radiation bath is damped. In the Fourier domain we get $1/(i\,\omega_{aa'} + \gamma)$, which may be written as

$$c_a c_{a'}^* \;\sim\; \frac{1}{1 + i\tan\beta} \;=\; \cos\beta\; e^{-i\beta}\,, \tag{2.9}$$

with angle β given by

$$\tan\beta = \frac{\omega_{aa'}}{\gamma}\,. \tag{2.10}$$

These expressions have the same form as the decoherence factor in Eqs. (2.7) and (2.8) for 'Hanle type' coherences between resonant transitions.

2.4. *Coherences in the final state*

The coherences in the final state are not independent of the coherences in the initial state, but they are linked according to the selection rules

$$m_f - m_{f'} \;=\; m_a - m_{a'}\,, \tag{2.11}$$

and

$$F_f - F_{f'} \;=\; F_a - F_{a'}\,. \tag{2.12}$$

The differences between the m and F quantum numbers of two interfering substates must thus be the same for the initial and final states. Equation (2.11) follows from a phase closure condition that must be obeyed for the product between the four geometrical ε factors that appear in each element of the coherency matrix $\mathbf{W}$ when we form the bilinear products between the elements of the Jones matrix of Eq. (2.3). In contrast the selection rule of Eq. (2.12) was not found from theoretical considerations, but it was demanded by the laboratory experiment; only when it was included it was possible to get good agreement between theory and experiment.

The decoherence suppression factor (depolarization) due to the difference in oscillation frequency between the initial substates is represented by the real part of Eq. (2.9), i.e., by the average of the expression and its complex conjugate. This average is $\cos^2\beta$. From symmetry considerations we expect that there should be a corresponding depolarization factor for the final-state coherences, the only difference being that $\omega_{aa'}$ in Eq. (2.10) should be replaced by $\omega_{ff'}$. Only when this depolarization factor is included in the theory we find agreement between theory and experiment.

3. Modeling the results of the laboratory experiment

3.1. *Experimental setup*

The experiment has been described in detail by Thalmann *et al.* (2006, 2009). It was done for potassium rather than sodium, since solid state tunable lasers are not available for the sodium wavelengths. As the K I D_2 7665 Å and the K I D_1 7699 Å lines have the same quantum number structure as the corresponding sodium lines, it is the same physics that is being tested in the two cases.

https://doi.org/10.1017/S1743921315004664 Published online by Cambridge University Press

The potassium is contained in a cross-shaped glass cell that was tailor-made for our experiment by the late Alessandro Cacciani, who had perfected the art of building such cells for use in magneto-optical narrow-band filter systems (Cacciani & Fofi 1978; Cacciani *et al.* 1997). Metallic potassium in the stem of the cell is heated to produce potassium gas at a temperature of 100° C at the cell center. The cell is filled with an argon buffer gas that suppresses diffusion of the potassium vapor toward the cooler entrance and exit windows, to prevent condensations that could make the windows opaque. While this type of cell is robust and easy to use, the buffer gas induces large collisional broadening and depolarization that have to be accounted for in the interpretation of the measurements.

The cross-shaped geometry of the cell allows us to explore the polarization properties of the light scattered at 90°. With polarizers in the expanded input laser beam any state of polarization can be chosen for the incident radiation. With a piezoelastic modulator, linear polarizer, and photomultiplier with lock-in amplifier in the output beam, any state of polarization (Stokes Q, U, or V) can be measured. Stepwise tuning of the laser wavelength allows the recording of polarized line profiles with mÅ resolution. With Helmholtz coils mounted on the cell arms a magnetic field with orientation in any of the three spatial directions can be imposed on the scattering region at the cell center.

While the accessible parameter space is thus very large, we will focus our attention on two cases: (1) Input radiation 100 % linearly polarized perpendicular to the scattering plane, while the Stokes I and Q profiles in the scattered beam are measured. (2) Input radiation 100 % circularly polarized, while the Stokes I and V profiles in the scattered beam are measured. In both cases the imposed magnetic field is oriented perpendicular to the scattering plane (transverse field case).

3.2. *Using D_2 to determine the free parameters*

While D_1 is a null line in terms of scattering polarization according to the standard recipe of Eq. (2.5), D_2 is a polarizing line because its excited (intermediate) state can be polarized. The D_2 line can be sufficiently well modeled with Eq. (2.5), because the contributions from coherences in the initial and final states are smaller than the polarization effects from the excited state by approximately a factor of 50. In contrast the D_1 Stokes Q profiles get *all* their polarization contributions from the new physical components of the extended theory, the coherences in the initial and final states. When using the experimentally determined polarized profiles of the D_2 line to fix the free parameters, their values will not be dependent on the way in which we try to extend standard scattering theory. These parameter values are subsequently used for testing the new, extended theory by comparing with the observed D_1 profiles with no further adjustable parameters.

There are two free parameters to be determined by D_2 fitting: the collision rate γ_c and the optical depth τ at the center of the D_1 line (which implies that it is 2τ at the D_2 line center because D_2 has twice as large oscillator strength). While the γ_c parameter plays a major role, the effect of τ is rather secondary.

Collisions affect the scattering polarization in three ways, all of which are governed by the γ_c parameter (according to idealized collision theory): (1) By increasing the effective damping parameter that governs the shape of the Φ_{ba} profiles in Eq. (2.2); (2) Through depolarization, reducing the magnitudes of the elements of the scattering Mueller matrix $\mathbf{M}$ with respect to the isotropic element M_{11}; (3) By increasing the partial overlap between the magnetic substates, thereby enhancing the coherence terms from the initial and final states.

The optical depth of the potassium gas in the cell arms must be finite, because if it were zero we would not get any scattered photons. It depends on the temperature of the cell: with higher temperature we evaporate more potassium from the metallic state. The

https://doi.org/10.1017/S1743921315004664 Published online by Cambridge University Press

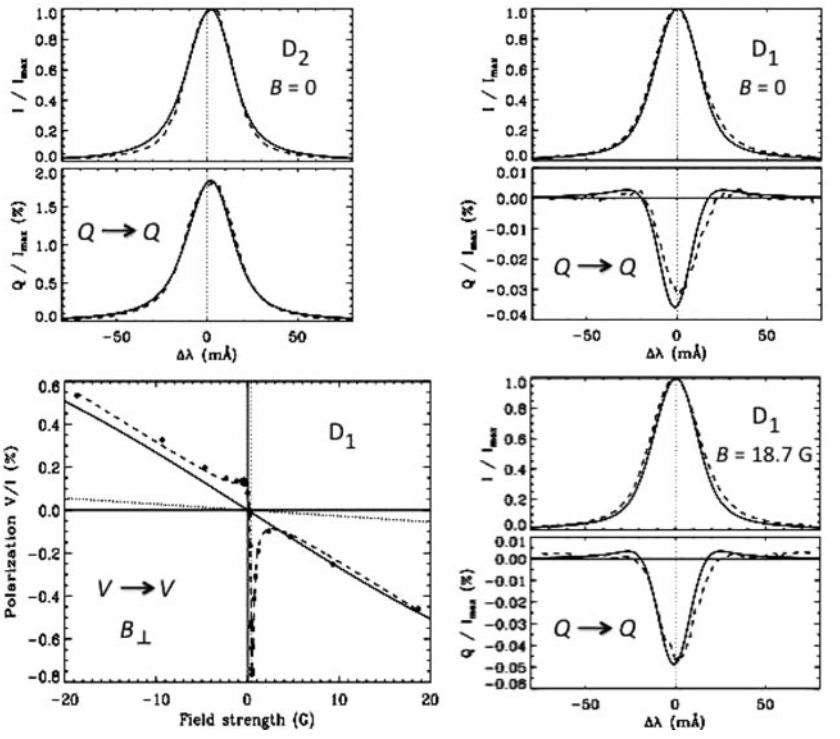

Figure 1. Comparison between observation (dashed curves) and theory (solid curves) for four various cases of 90° scattering at potassium gas. The top set of panels for the Stokes I and Q line profiles refer to non-magnetic scattering of linear polarization ($Q \rightarrow Q$) in the D_2 (left panels) and D_1 (right panels) lines. The D_2 theoretical fit serves to fix the two free parameters of the model, collision rate γ_c and optical depth τ. With the old quantum scattering recipe of Eq. (2.5) we would expect null results for Stokes Q of the D_1 line. The entire Q profile is produced by coherences in the initial and final states. When a transverse magnetic field is introduced the relative profile shapes remain the same, but the Q amplitude increases, as indicated in the panels to the lower right. This enhancement can be shown to be due to magnetically induced dichroism not related to the scattering process. The diagram to the lower left shows the results for D_1 scattering of circular polarization ($V \rightarrow V$), when the strength of the transverse field is varied. What is plotted is the fractional circular polarization V/I of the scattered radiation, defined as wavelength-integrated Stokes V divided by integrated Stokes I. With the old quantum recipe of Eq. (2.5) the dotted line is obtained, which has a slope an order of magnitude smaller than that of the solid line. This shows that the scattered circular polarization is dominated by the effects of coherences in the initial and final states. The sharp negative peak that is centered at 0.43 G is due to the Earth's magnetic field. In the milligauss range around this value the orientation of the residual, uncompensated field varies dramatically in a way that is not sufficiently known to allow modeling.

cell temperature is chosen to give us enough scattered photons to make it possible to record tiny polarization amplitudes (with a sensitivity in the 10^{-5} range), while keeping the optical depth less than unity to avoid effects of multiple scattering and deformed line profiles (through self-absorption).

The panels to the upper left of Fig. 1 show the scattered Stokes I and Q profiles (normalized to the maximum value of the I profile) found by laser tuning through the D_2 line in the non-magnetic case when the incident beam is 100 % linearly polarized perpendicular to the scattering plane (the direction in which positive Q is defined, which means that the input $Q/I = 1$). We refer to this combination of input-output polarization

https://doi.org/10.1017/S1743921315004664 Published online by Cambridge University Press

as $Q \rightarrow Q$ scattering. The theoretical curves (solid) provide a nearly perfect fit to the experimental curves (dashed) with the use of the values $\gamma_c = 90\gamma$ and $\tau = 0.25$ for the two free parameters (where γ is the radiative damping width). Thermal Doppler broadening corresponding to the cell temperature of 100° C has been applied, but there is no additional spectral smearing. While the value of γ_c is fixed by the fit to the observed Stokes Q amplitude, the value of τ is determined by the fit of the line widths. With larger τ the theoretical profiles would be too wide, while with smaller τ there would be a need for an additional ad hoc spectral smearing to account for the observed line widths. It turns out that the value of τ that accounts for the line widths also explains the magnetic-field dependence of the Stokes Q profile for the D_1 line (see below).

3.3. *Comparison between theory and observation for D_1 scattering*

Since the environmental cell conditions were identical for the D_2 and D_1 recordings, the values of the fit parameters γ_c and τ that have been determined with the D_2 data can be used for the theoretical calculation of D_1, with no further parameter fitting. In the upper right-hand corner of Fig. 1 we show the results for the identical experimental setup as used for the mentioned D_2 recording, namely $Q \rightarrow Q$ scattering for the non-magnetic case. As before the theoretical and experimental results are represented by the solid and dashed curves, respectively. Also here the fit is nearly perfect, although no parameter fitting has been used. We notice in particular that the scattered Q polarization is negative (opposite to the D_2 case), implying linear polarization *parallel* to the scattering plane, but with a polarization amplitude that is about 50 times smaller than that of D_2.

The small systematic shift toward the right of the dashed Q curve relative to the solid one is not due to a deficiency of the theory, but has to do with the time constant used for the lock-in amplifier when recording exceedingly weak polarizations that demand a polarimetric precision in the 10^{-5} range. To reach this precision we had to apply the largest possible temporal integration (analog time constant) that is compatible with the stepwise wavelength tuning rate of the laser without producing excessive wavelength smearing and shift. This choice of time constant has resulted in the mentioned Q curve shift, which is about 2.8 mÅ or 1.7 tuning steps.

The fundamental importance of the non-magnetic $Q \rightarrow Q$ scattering diagram for D_1 is that it unambiguously reveals the signatures of neglected physics that have been missing in previous scattering theory. If we would use the quantum recipe of Eq. (2.5) we would get zero scattered Q for all wavelengths. The entire profile, computed with the use of Eq. (2.6), has its source in the coherences in the initial and final states.

When we vary the strength of an imposed transverse magnetic field (oriented perpendicular to the scattering plane) we find that Stokes Q has a quadratic dependence on field strength, as one expects for the transverse Zeeman effect. The theoretical modeling shows that this field dependence comes almost exclusively from magnetically induced dichroism in the potassium gas and not from the scattering process. In the limit of vanishing optical depth τ there would be no significant field dependence (over the explored field-strength range). With our value $\tau = 0.25$ that was determined exclusively with D_2 data by fitting the widths of the I and Q profiles it is possible to reproduce the observed field dependence for Stokes Q of the D_1 line.

In the lower right-hand corner of Fig. 1 we show the Stokes I and Q profiles for the case when the strength of the transverse field is 18.7 G. While the relative profile shapes are almost identical to those of the non-magnetic case, we notice that the scales used for the Q polarization are significantly different in the two cases. The dichroism enhances the magnitude of the negative Q polarization.

https://doi.org/10.1017/S1743921315004664 Published online by Cambridge University Press

In the diagram to the lower left of Fig. 1 we finally show the field dependence of $V \rightarrow V$ scattering for D_1. As before, the field orientation is transverse (perpendicular to the scattering plane), but now the input beam is 100 % right-handed circularly polarized, and we measure the degree of circular polarization in the scattered beam for a sequence of field strengths. Instead of showing line profiles we here give for each field strength the fractional circular polarization V/I of the scattered radiation defined as the integrated Stokes V profile divided by the integrated Stokes I profile. The observations are represented by the filled circles and the dashed fit curve, while the theory is represented by the slanted solid line.

If we disregard the innermost part in the weak field-strength range between -1 and $+2$ G, the agreement between the solid and dashed curves is excellent, they have the same slopes. We again stress that no free model parameters have been used (since the values of γ_c and τ were already fixed by fitting the D_2 data). In contrast to the $Q \rightarrow Q$ scattering case magnetically induced dichroism by transverse magnetic fields have no effect on the fractional V/I polarization in the $V \rightarrow V$ scattering case. All the polarization effects have their origin in the D_1 scattering process.

For comparison the slightly slanted dotted line has been obtained with the old quantum recipe of Eq. (2.5). It has a slope that is an order of magnitude smaller than that of the solid line. The source of this small slope is quantum interferences in the upper, excited state. Without these quantum interferences we would get null results for all field strengths. Comparison with the solid line shows however that the dominating source of circular polarization in the scattered radiation is coherences in the initial and final states, while the upper-state coherences play a minor, secondary role.

The spectacular sharp negative V/I peak that is located at a field strength of 0.43 G is beyond the reach of our current theoretical modeling. It can be understood as due to the Earth's magnetic field, which has a downward vertical component of approximately this magnitude. It gets compensated when our imposed magnetic field has an upward component of this magnitude. The terrestrial magnetic field is however inclined, so when the vertical component gets compensated, the residual field becomes horizontal with an azimuth that is not well known for our experimental setup. In the milligauss range around the 0.43 G value the orientation of the residual magnetic field will vary dramatically, in a way that we cannot reproduce for modeling purposes. The observed sharp negative peak however reveals an enormous sensitivity of the scattered circular polarization to the field orientation in the milligauss regime. This fascinating behavior needs to be explored in future experiments that should be carried out in a magnetically clean environment.

4. Concluding remarks

The world of quantum physics is richly structured in ways that are often not fully understood. The physics of polarized scattering at multi-level atomic systems has important applications, but the theories used have been poorly tested. The D_1 lines of sodium, potassium, lithium, and ionized barium are ideal for such test purposes, since with traditional scattering theory D_1 can be regarded as unpolarizable. When the theory finally got experimentally tested with scattering at potassium gas, it failed the test. A rich polarization structure was revealed where the theory predicted null results. Quantum scattering was found to have a far richer coherence structure than previously believed.

In the present paper we identify the physical ingredients that have been missing (coherences in the initial and final states) and show how they can be included in a self-consistent way in an extended theory, which is then used to reproduce the experimental results in great quantitative detail. Although the theory is sufficiently well defined to successfully

https://doi.org/10.1017/S1743921315004664 Published online by Cambridge University Press

model the laboratory experiment, it has not yet been formulated in a way that is general enough for integration in a radiative-transfer formalism that can be used with confidence for the interpretation of solar observations.

The further refinement of the theory should be guided by improved laboratory experiments. Two major improvements will be needed: (1) Implementation of D_1 scattering under collisionless conditions. At present the experimental results are heavily affected by the large collision rate induced by the buffer gas in the vapor cell. We need a setup that does not make use of a buffer gas. (2) Making the test environment magnetically clean to allow us to explore the scattering behavior in the milligauss regime. The present experiment has revealed that there is an enormous sensitivity of the scattering polarization to the field orientation in the milligauss range. This behavior needs to be fully understood and consistently included in a complete scattering theory.

It has been widely believed that the physical foundation of quantum scattering is well understood, and that the remaining task is to properly apply the theory to complex environments like the Sun. The development of any complex theory however always needs to be guided by experiment. Using polarized scattering we have confronted quantum theory with an experiment in a previously untested domain and have found that the theory fails. This failure has however revealed to us that quantum systems may often have a far richer coherence structure than previously believed. It also indicates the direction to go in our quest to understand this hitherto poorly explored aspect of nature.

References

Belluzzi, L. & Trujillo Bueno, J. 2013, *ApJ* 774, L28

Cacciani, A. & Fofi, M. 1978, *Solar Phys.* 59, 179

Cacciani, A., Moretti, P. F., & Rodgers, W. E. 1997, *Solar Phys.* 174, 115

Casini, R. & Manso Sainz, R. 2005, *ApJ* 624, 1025

Casini, R., Landi Degl'Innocenti, E., Landolfi, M., & Trujillo Bueno, J. 2002, *ApJ* 573, 864

Gandorfer, A. M., Steiner, P., Povel, H. P., *et al.* 2004, *A&A* 422, 703

Hanle, W. 1924, *Z. Phys.*, 30, 93

Kerkeni, B. & Bommier, V. 2002, *A&A* 394, 707

Klement, J. & Stenflo, J. O. 2003, in: J. Trujillo-Bueno & J. Sanchez Almeida (eds.), *Solar Polarization 3*, ASP Conf. Series 307 (San Francisco: ASP), p. 278

Landi Degl'Innocenti, E. 1998, *Nature* 392, 256

Landi Degl'Innocenti, E. & Landolfi, M. 2004, *Polarization in spectral lines*, Kluwer, Dordrecht

Povel, H. 1995, *Optical Engineering* 34, 1870

Povel, H. P. 2001, in: G. Mathys, S. K. Solanki, & D. T. Wickramasinghe (eds.), *Magnetic Fields Across the Hertzsprung-Russell Diagram* , ASP Conf. Series 248 (San Francisco: ASP), p. 543

Stenflo, J. O. 1994, *Solar magnetic fields - Polarized radiation diagnostics*, Kluwer, Dordrecht

Stenflo, J. O. 1998, *A&A* 338, 301

Stenflo, J. O. 2015, *ApJ* 801, 70

Stenflo, J. O. & Keller, C. U. 1996, *Nature* 382, 588

Stenflo, J. O. & Keller, C. U. 1997, *A&A* 321, 927

Stenflo, J. O., Gandorfer, A., & Keller, C. U. 2000a, *A&A* 355, 781

Stenflo, J. O., Keller, C. U., & Gandorfer, A. 2000b, *A&A* 355, 789

Thalmann, C., Stenflo, J. O., Feller, A., & Cacciani, A. 2006, in: R. Casini & B. W. Lites (eds.), *Solar Polarization 4*, ASP Conf. Series 358 (San Francisco: ASP), p. 323

Thalmann, C., Stenflo, J. O., Feller, A., & Cacciani, A. 2009, in: S. V. Berdyugina, K. N. Nagendra, & R. Ramelli (eds.), *Solar Polarization 5: In Honor of Jan Stenflo*, ASP Conf. Series 405 (San Francisco: ASP), p. 113

Trujillo Bueno, J., Casini, R., Landolfi, M., & Landi Degl'Innocenti, E. 2002, *ApJ* 566, L53